Control Engineering Practice 150 (2024) 106010

Contents lists available at ScienceDirect

Control Engineering Practice

journal homepage: www.elsevier.com/locate/conengprac

Control strategies for mode switching of a large marine two-stroke engine equipped with exhaust gas recirculation and turbocharger cut-off systems

Daoyi Lu [a,1], Gerasimos Theotokatos [b,*,1], Keying Cui [c]

[a] Marine Engineering College, Dalian Maritime University, Dalian, 116026, China
[b] Maritime Safety Research Centre, Department of Naval Architecture, Ocean and Marine Engineering, University of Strathclyde, Glasgow, G4 0LZ, UK
[c] Dalian Marine Diesel Co Ltd., Dalian, 116021, China

ARTICLE INFO

Keywords:
Two-stroke marine engine
Exhaust gas recirculation system
Turbocharger cut-off
Dynamic simulation
Control strategies

ABSTRACT

To meet the stringent nitrogen oxides emissions regulations, the recent marine two-stroke engines are equipped with exhaust gas recirculation (EGR) systems. Crossing the boundaries of exhaust control areas requires switching between the engine operating modes associated with the activation or deactivation the EGR system, which imposes challenges to the engine operation. This study aims to develop and numerically test effective control strategies for improving the mode switching of marine two-stroke engines with EGR systems. The investigated engine dynamic model is developed by integrating a zero-dimensional thermodynamic model developed in GT-POWER and the control model developed in MATLAB/Simulink. This model is first validated against the experimentally measured engine performance parameters, and subsequently employed to simulate the engine dynamic operation with mode switching. The simulation results are assessed to quantify the impact of several control strategies on the engine performance. The derived perrformannce parameters time variations demonstrate that the deactivation of the EGR branch and the small engine–turbocharger result in exceeding the manufacturer limits at high loads and increasing the fuel consumption. The proposed load-based control strategies, which employ load thresholds and time delays for the control of the EGR and turbocharging systems activation/deactivation, are proved effective, as the engine performance parameters are retained within their limits and fuel consumption penalties are minimised. This study provides insights for developing the control of the marine engines after-treatment systems, hence contributing towards enhancing shipping sustainability.

1. Introduction

To comply with the stringent regulations for nitrogen oxides (NOx) emissions introduced by the International Maritime Organisation (IMO) (IMO, 2008), marine engines manufacturers have developed and integrated into their engines after-treatment systems for either exhaust gas recirculation (EGR) or selective catalytic reduction (SCR) (MAN, 2015; Nakagawa, Ito, & Edo, 2019; Schneiter, 2015). The former recirculates the exhaust gas into the engine cylinders reaching NOx emissions reduction by up to 80% (Lou, Lou, Wang, Fang, & Zhang, 2021; Nakagawa, Onishi, Nakao, Hosono, & Nishiyama, 2016), whereas the latter employs catalysts to achieve NOx emissions reduction above 90% (Liu et al., 2022; Vignesh & Ashok, 2020).

The SCR systems are associated with limitations pertaining to their considerable volume and thermal inertia. The EGR systems layouts are less challenging, hence they have been implemented on marine engines since 2005 (MAN, 2008). Several EGR systems have been installed on newbuilt ships (Hiraoka et al., 2016; Kaltoft & Preem, 2013; MAN, 2020; Mandra, 2022). The EGR impact on the NOx emissions reduction is reported in the pertinent literature (Hountalas, Raptotasios, & Zannis, 2013; You, Liu, Wang, Wang, & Xu, 2020; Zheng, Reader, & Hawley, 2004), with the main contributors being associated with: (a) the thermal effects that increase the in-cylinder working medium specific heat, hence reducing the combustion temperature, and: (b) the dilution effects resulting in reduced in-cylinder oxygen concentration, thus reducing the combustion rate.

To address the contradictory engine requirements when operating with the EGR system activated or deactivated, marine two-stroke engines with single or multiple turbochargers employ bypass valves at their turbocharger turbine(s) and cylinders (Lu, Theotokatos, Zhang, Zeng, & Cui, 2022b; MAN, 2015). Controlling these valves allows for avoiding turbocharger over-speeding at high loads and improving the turbocharger system matching when the EGR system is activated. For such a marine engine, Wang, Zhou, Feng, and Zhu (2017) reported NOx reduction by 76% accompanied by increased fuel consumption.

* Corresponding author.
E-mail address: gerasimos.theotokatos@strath.ac.uk (G. Theotokatos).
[1] These authors contributed equally to this study.

https://doi.org/10.1016/j.conengprac.2024.106010
Received 23 October 2023; Received in revised form 23 June 2024; Accepted 24 June 2024

Abbreviations	
A/C	Air cooler
BBV	Blower bypass valve
BSFC	Brake specific fuel consumption
BTV	Blower throttle valve
CBV	Cylinder bypass valve
CCV	Compressor cut-off valve
DEM	Dynamic engine model
EGR	Exhaust gas recirculation
EGRBP	EGR system with exhaust gas bypass
EGRTC	EGR system with turbocharger cut-off
NOx	Nitrogen oxides
SMCR	Specified maximum continuous rating
SOV	EGR shut-off valve
T/C	Turbocharger
TCV	Turbine cut-off valve
WMC	Water mist catcher

Wang et al. (2020) reported that similar EGR and cylinder bypass flow rates can improve the engine performance. Wang, Zhang, Qian, and Deng (2022) argued that the cylinder bypass opening results in higher exhaust gas oxygen concentration, posing limitations in the NOx emissions reduction. Lu, Theotokatos, Zhang, Zeng, and Cui (2022a) parametrically investigated the impact of the EGR and cylinder bypass valves control on a marine two-stroke engine brake specific fuel consumption (BSFC) and NOx emissions trade-offs, defining their optimal values. Alegret, Llamas, Vejlgaard-Laursen, and Eriksson (2015) employed mean value modelling for a marine diesel engine with EGR system to numerically test control strategies. Stoumpos and Theotokatos (2020) parametrically optimised a marine four-stroke engine equipped with an EGR system identifying the EGR and cylinder bypass valves settings to achieve compliance with the Tier III NOx emissions standards.

As the number of giant ships, such as ultra-large oil tankers, ore carriers, and container ships, has increased the last decade (Loganx, 2019), marine two-stroke engines equipped with two or more turbochargers connected in parallel are used for these ships propulsion. An alternative design for these engines to achieve Tier III NOx emissions compliance includes the main turbocharger, the EGR system and the cut-off turbocharger, as reported in Kaltoft and Preem (2013).

Lu et al. (2022b) investigated the turbocharging system matching for a marine engine of this type proposing an effective matching procedure. Lu et al. (2022a) parametrically optimised and comparatively assessed marine engines with EGR systems of these two types. It was demonstrated that the engine with cut-off turbocharger exhibited higher efficiency for the same NOx emissions reduction. However, the mode switching (from Tier II to III and vice versa) is expected to raise challenges for the engine and its sub-systems, pertaining to the main turbocharger over-speeding, exceeding the manufacturer limits at high loads, time delays to achieve steady state conditions, and fuel consumption penalties. This underpins the need to investigate the transient response of marine engines with EGR system and cut-off turbocharger, as well as to develop effective control strategies for mode switching.

This study aims to develop control strategies to improve the mode switching for a large marine two-stroke diesel engine with the EGR system and cut-off turbocharger (EGRTC engine henceforth) through numerical investigation. The considered case studies include the switching from the Tier II mode to the Tier III mode and vice versa. Several control strategies are assessed based on the derived simulation results considering the response and limits of key performance parameters. The most effective control strategies for these mode switching cases are identified.

The novelty of this study stems from: (1) the development of the mode switching control strategies for the EGRTC engine leading to the lowest impact to fuel consumption increase as well as retaining the engine parameters within the permitted limits; (2) the development of a detailed dynamic model integrating the thermodynamic model of the investigated engine along with its sub-systems (EGRTC system, parallel turbocharging system), and the control strategy model that represents the engine and EGR control systems; (3) the numerical study of the mode switching for the investigated marine engine equipped with the EGRTC system.

Table 1
Investigated engine main particulars.

Parameter	Unit	Value
Cylinders number	–	7
Bore	mm	800
Stroke	mm	3720
Speed at SMCR point	r/min	58
Power at SMCR point	kW	24,440
Large T/C maximum pressure ratio	–	5.5
Large T/C maximum speed	r/min	15,000
Large T/C compressor diameter	m	0.7
Small T/C maximum pressure ratio	–	5.5
Small T/C maximum speed	r/min	20,820
Small T/C compressor diameter	m	0.5
NOx emissions compliance	–	Tier II/III
NOx reduction technology	–	EGR

2. Investigated engine

This study investigates the marine two-stroke diesel engine 7G80ME from MAN Energy Solutions, which is used as the propulsion engine of very large oil tankers and ore carriers (MAN, 2018). This engine complies with the IMO Tier III NOx emissions standards. Table 1 presents its main specifications at the Specified Maximum Continuous Rating point (SMCR).

The engine is equipped with EGR system and cut-off turbocharger (EGRTC). Its turbocharging system consists of one large turbocharger (large T/C) and one small turbocharger (small T/C or cut-off T/C) connected in parallel. The large T/C is the engine main turbocharger, whereas the small T/C can be switched on or off depending on the engine operating mode. The engine can operate in two modes, referred as Tier II and Tier III henceforth, which meet the respective IMO NOx emissions standards. The engine layout and the controlled components are shown in Fig. 1.

For the Tier II mode, the small T/C is activated with the turbine cut-off valve (TCV) and compressor cut-off valve (CCV) being switched on (fully open), the EGR branch is deactivated with the blower throttle valve (BTV) and EGR shut-off valve (SOV) being switched off, whereas the blower bypass valve (BBV) is switched on. For the Tier III mode, the small T/C is cut off with the TCV and CCV being switched off, the EGR branch is activated with the SOV and BTV being switched on, whereas the BBV is switched off. The large T/C is activated in both modes.

Apart from the Tier II and Tier III operating modes, an additional mode, denoted as Tier II-L, with both the small T/C and the EGR system deactivated is considered herein. This is required as an intermediate step for the Tier II to Tier III mode switching and vice versa. The switching sequence between these three operating modes is shown in Fig. 2. The engine shop trials revealed that the engine valves switching from their fully open to fully closed positions (and vice versa) lasted about 10 s. This value was considered herein.

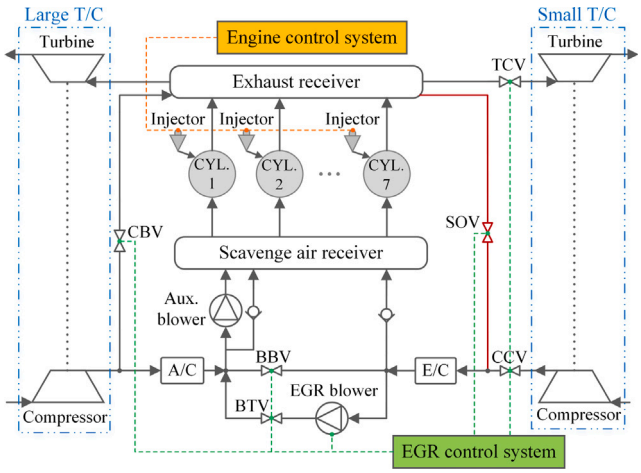

Fig. 1. Investigated engine layout.

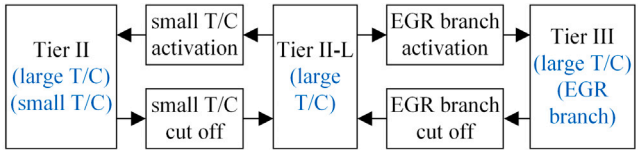

Fig. 2. Engine operating modes and mode switching sequence.

3. Engine model development and validation

3.1. Methodology

The model development and validation methodology consists of five steps, which are illustrated in the flowchart shown in Fig. 3. These steps are briefly described as follows.

- **Step 1**: The steady-state engine model (SEM) of the engine and its EGR system was developed in the GT-POWER software (Gamma, 2016c). The SEM is calibrated to ensure that the maximum percentage errors in key performance parameters (compared to their experimentally measured values) such as cylinder pressure, fuel consumption, scavenging receiver pressure and temperature, exhaust gas receiver pressure and temperature, at steady-state conditions, are within acceptable limits according to ISO15550, as reported in Jeon and Theotokatos (2024).
- **Step 2**: The SEM was validated against experimentally measured parameters for five engine loads, in specific, 15%, 25%, 50%, 75% and 100%.
- **Step 3**: The control system model for the engine as well as its turbocharging and EGR subsystems (shown in Fig. 1) was developed in MATLAB/Simulink.
- **Step 4**: The SEM (GT-POWER) and the control system model (Simulink) were interconnected to develop the dynamic engine model (DEM).
- **Step 5**: The DEM was employed to simulate scenarios with dynamic conditions, the results of which were used for its verification.

3.2. Engine and EGR systems modelling

The engine is modelled using a combined zero/one-dimensional modelling approach. The developed model includes blocks (sub-models) for the following engine components: scavenge air receiver, air cooler, auxiliary blower, cylinders, exhaust gas receiver, T/Cs.

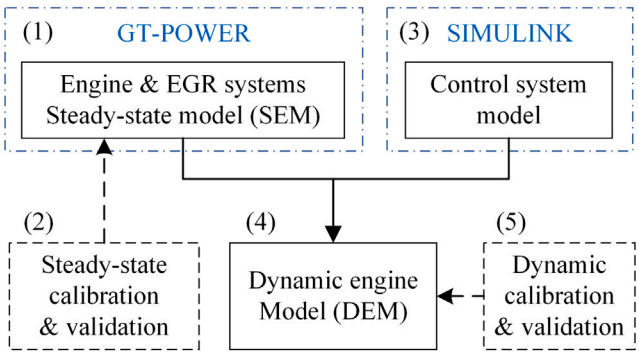

Fig. 3. Model development and validation methodology flowchart.

The Direct-Injection Diesel Multi-Pulse Combustion Model (Gamma, 2016a) (DI-Pulse model) is employed for representing the engine combustion process. This is a predictive combustion model, which adopts only one set of parameters for the whole engine operating envelope (Park, Cho, Park, & Song, 2017; Wang et al., 2020). The DIPulse model employs the main unburned zone that contains the in-cylinder contents at the beginning of the closed cycle, the spray unburned zone that contains the injected fuel and entrained gas, as well as the spray burned zone that contains the combustion products. The working medium temperature and composition are calculated for each zone.

The model calibration involves four constants that impact the following parameters: entertainment rate, ignition delay, premixed combustion rate, and diffusion combustion rate. The Advanced Direct Optimiser (ADO) that is part of GT-SUITE was employed for these four constants calibration. The non-dominated sorting genetic algorithm (NSGA III) was employed to estimate a single set of these four constants values by minimising the objective function consisting of the root mean square error for the in-cylinder pressure and BSFC weighted for the four investigated loads. The detailed description of the DI-Pulse model and its calibration process is provided in the authors' previous studies (Lu et al., 2022a, 2022b).

The other engine cylinder processes are modelled by well-established sub-models and formulae. The Woschni empirical formula (Woschni, 1967) is employed to represent the cylinder heat transfer. The friction mean effective pressure is calculated using the Chen–Flynn empirical formula (Chen & Flynn, 1965). A two-zone model (Lu et al., 2021) is employed to represent the cylinder scavenging process, for which the relationship between the in-cylinder residual rate and the exhaust gas residual rate is provided as input. The quasi-steady-state adiabatic flow equations are used to calculate the scavenging port and exhaust valve mass flow rates, considering as input the respective equivalent area profiles (versus crank angle).

The developed model employs several input parameters, such as, the fuel injection and the exhaust valve timing. Interpolation is employed to estimate these parameters as function of the engine load, thus allowing for simulating the complete engine operating envelope for both steady state and dynamic conditions.

The engine scavenge air and exhaust receivers were modelled by employing a zero-dimensional method based on the conservation of mass, and energy (Gamma, 2016b). The air cooler was modelled as multiple parallel ducts with an appropriate heat transfer coefficient being calibrated to adequately predict the air cooler outlet temperature. The auxiliary blower and EGR blower were modelled by employing their performance maps (Kaltoft & Preem, 2013; Shen, 2020). The EGR system valves were modelled based on the characteristics of solenoid-actuated valves (Gamma, 2016b), with their opening and closing profiles being defined as function of time. These valves are controlled via control signals, with their close and open positions

Table 2
Calibrated EGR blower speed and predicted NOx emissions.

Engine load (%)	15	25	50	75	100
Measured NOx emissions (g/kWh)	n/a	4.46	4.10	2.40	2.56
Predicted NOx emissions (g/kWh)	4.46	4.47	4.10	2.42	2.56
Predicted EGR rate (%)	33.6	34.7	32.8	33.4	25.8
Calibrated EGR blower speed (r/min)	4380	6150	7130	6920	4690

corresponding to 0 and 1, respectively, whereas their opening or closing starts when the control signal switches between 0 and 1 or vice versa.

The T/Cs turbines and compressors were modelled by using their respective performance maps (Lu et al., 2022b; Shen, Zhang, Yang, & Jia, 2020). The T/C shaft speed was calculated by integrating the angular momentum conservation equation.

The engine shaft speed N_e is calculated according to the following equation that was derived by the angular momentum conservation:

$$\frac{dN_e}{dt} = \frac{30}{\pi}\frac{\eta_{sh}M_e - M_p}{I_e + I_{sh} + I_p} \tag{1}$$

where η_{sh} is the shafting system efficiency, M_e is the engine torque (N m), I_e, I_{sh} and I_p represent the engine, shafting system, and propeller inertia (kg m^2).

The propeller torque M_p is calculated using the following equation:

$$M_p = k_Q \rho {N_p}^2 {D_p}^5 \tag{2}$$

where k_Q is the propeller torque coefficient, ρ is the seawater density (kg/m^3), D_p is the propeller diameter (m), and N_p denotes the propeller speed (r/min), which is the same with the engine shaft speed for direct drive propulsion systems (employed for marine two-stroke engines).

The NOx emissions are calculated according to the extended Zeldovich mechanism (Bowman, 1973; Rao & Honnery, 2013) considering the in-cylinder pressure, temperature, and oxygen concentration time variations. The in-cylinder oxygen concentration depends on the recirculated exhaust gas mass flow, which is adjusted by controlling the EGR blower speed.

The EGR blower speed was determined by employing an iterative process targeting to achieve the experimentally measured NOx emissions at the Tier III mode. Table 2 presents the derived results for the EGR blower speed. For 15% load, the measured NOx emissions value at 25% load was employed due to the lack pertinent data.

3.3. Control system modelling

The engine control system model consist of blocks for the control of the fuel injected amount, the auxiliary blower, the EGR blower, as well as the EGR and T/C system valves. This study does not involve the modelling of the control for the engine start and stop. The modelled control functions are shown in Fig. 4.

The fuel controller includes a proportional–integral–differential (PID) governor, which employs as input the actual and ordered shaft speeds, whereas it provides as output the fuel index. This module also includes the torque and scavenging pressure limiters (according to the engine manufacturer), with the input being the engine speed in the former and the scavenge air pressure in the latter. The fuel index (output of the limiters block) is used to calculate the injected fuel mass for each cylinder, which is provided as input to the GT-POWER model.

Marine two-stroke diesel engines are equipped with auxiliary blowers to facilitate the cylinders air flow at low loads. The auxiliary blower controller model controls the auxiliary blower activation/deactivation and adjusts its rotational speed considering as input the scavenge air pressure values for the blower activation and deactivation.

The EGR blower controller model is responsible for deactivating (Tier II mode) or activating the EGR blower and control its rotational

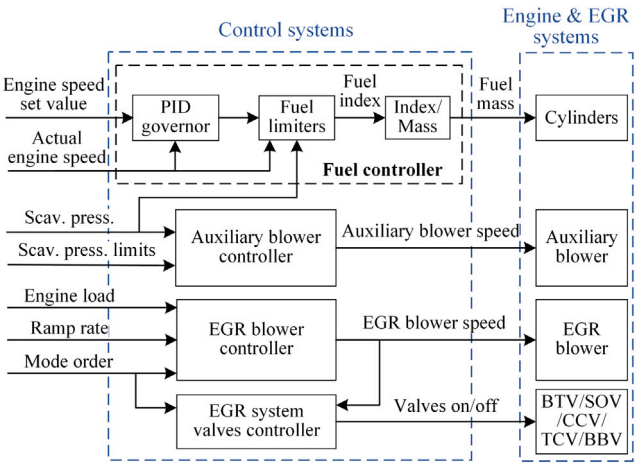

Fig. 4. Engine control model schematic.

speed (Tier III mode). The ordered mode (Tier II or Tier III) and the engine load are employed as input; the former for deactivation/activation; the later to adjust the EGR blower speed (using interpolation considering the values listed in Table 2). The acceleration and deceleration rates of the EGR blower speed are considered to investigate the impact of EGR blower activation/deactivation duration on the engine performance parameters.

To activate or deactivate the small T/C and the EGR branch, the EGR system valves controller model controls the opening and closing of the EGR blower throttle valve (BTV), the EGR shut-off valve (SOV), the compressor cut-off valve (CCV), the turbine cut-off valve (TCV) and the EGR blower bypass valve (BBV). The controller outputs a logic signal (0 or 1). These valves are classified into the following two groups: (1) the CCV, the TCV and the BBV, to control the small T/C activation/deactivation; (2) the BTV and the SOV, to control the EGR branch activation/deactivation. The valves in the same group will receive the same command and operate simultaneously (open or close).

To prevent the scavenging air flowing into the exhaust receiver through the EGR branch, the valves should only be opened when the BTV pressure difference is positive. As an alternative measure to prevent air back-flow, the BTV and SOV are kept closed when the EGR blower speed is lower than the threshold of 1000 rpm; the latter was identified by simulation runs.

3.4. Dynamic engine model

The GT-POWER model layout for the engine and its EGR system engine (SEM) is presented in Fig. 5. This model employs the pre-set fuel injection mass and engine speed to simulate steady-state conditions. The GT-POWER and the control systems Simulink model were interconnected forming the dynamic engine model (DEM). The integrated engine model runs from the MATLAB/Simulink environment.

The input parameters to the Simulink model are the engine torque and the scavenge air receiver pressure. The input signals to the GT-POWER model include the following: engine speed, EGR blower speed, open/close signals for BTV, SOV, CCV, TCV, and BBV. The engine speed is calculated by the Simulink model. The injected fuel mass is calculated by the fuel controller module of the Simulink model, and is provided as input into the GT-POWER model. The engine torque is calculated by the GT-POWER model and is fed back to the Simulink model.

3.5. Model validation

Table 3 illustrates the overview of the performed validation tests for the DEM. The validation at the steady-state conditions was performed

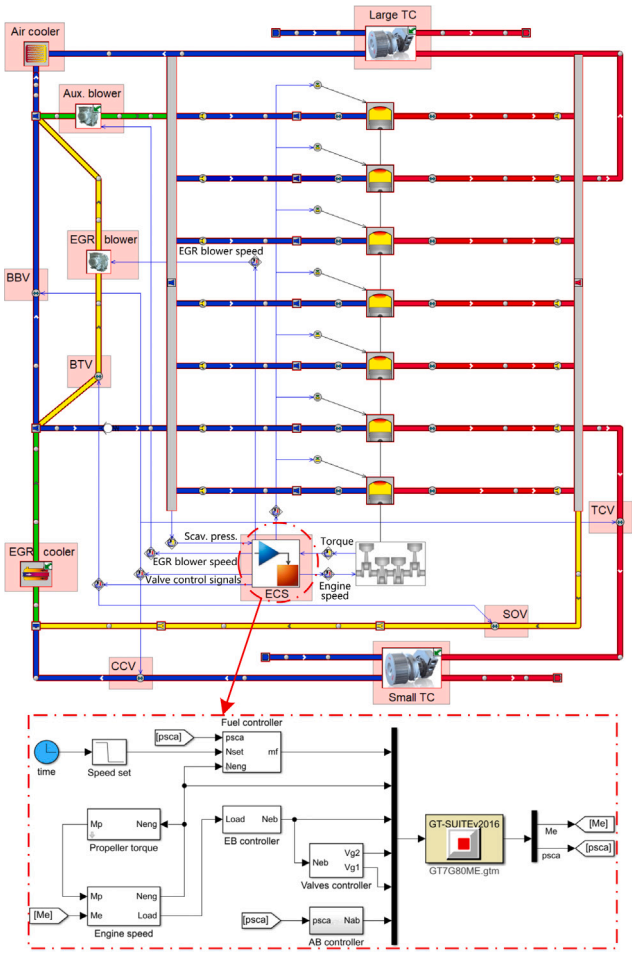

Fig. 5. Integrated engine model in GT-POWER and MATLAB/Simulink.

Table 3
DEM validation tests summary.

Mode	Load/change (%)	Scope
Tier II	10–100 (step: 5)	Validation at steady-state conditions
Tier III	26 to 42 (ramp increase)	Validation at transient conditions

for the Tier II mode (EGR branch deactivated, small T/C activated). The validation at transient conditions were performed for the Tier III mode (EGR branch activated, small T/C deactivated). The model validation was carried out by considering the shop trials data for the investigated engine and transient response data published in Nielsen, Blanke, Eriksson, and Vejlgaard-Laursen (2017, 2018). The DEM validation at steady state conditions considered loads between 10% and 100% with increment of 5%; in total 19 operating points were simulated. The measured parameters for 15%, 25%, 50%, 75% and 100% loads from the engine shop trials were employed to validate the simulation results.

Fig. 6 presents the derived steady state simulation results along with their respective measured values for the in-cylinder maximum pressure and compression pressure, the brake specific fuel consumption (BSFC), the NOx emissions, the scavenge air receiver pressure and temperature, the exhaust gas receiver pressure and temperature, as well as the in-cylinder pressure diagrams. The corresponding percentage errors were found less than 3.6%, with the maximum error values exhibited for the exhaust gas temperature. The estimated errors were found within the acceptable limits according to ISO15550 as reported in Jeon and Theotokatos (2024); in specific, 5% for exhaust gas temperature and

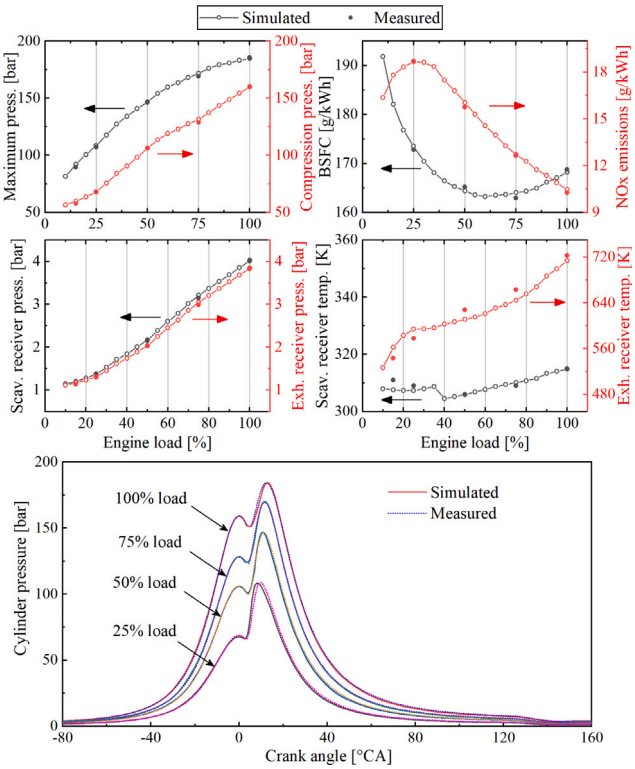

Fig. 6. Validation results at steady state conditions for the Tier II mode.

pressure, 2% for the T/C speed, 3% for fuel consumption. It is also deduced that the derived parameters variations with the engine load are continuous and reasonable, whereas the impact of the auxiliary blower activation on the scavenge air receiver temperature at low loads (less than 40%) is adequately captured. Based on the presented results, it is inferred that the DEM adequately represents the engine steady state conditions for the Tier II mode.

The experimentally measured engine speed time variations reported in Nielsen et al. (2017, 2018) for a similar marine diesel engine (MAN B&W 6S80ME with SMCR speed 74 rpm) were employed to validate the DEM at transient conditions. To reduce exhaust smoke formation at the Tier III mode, Nielsen et al. (2018) proposed EGR control algorithms with fixed-gain feedback (FGF) or adaptive feedforward (AFF) and several fuel limiter functions (air/fuel ratio limiter; oxygen/fuel limiter based on oxygen concentration estimation model; oxygen/fuel limiter based on oxygen sensor). These algorithms testing was performed for a container vessel main engine operating under load increase conditions from 26% (35 rpm) to 42% load (50 rpm). The measured engine speed time variations are shown in Fig. 7 (bottom). The tested algorithms achieved the engine speed convergence within 90–110 s from the load change order (at the 50th s). Considering that the measured data were obtained under stricter fuel limit conditions, this study calibrated the governor to achieve engine speed convergence within 90 s.

Fig. 7 (top) presents the predicted engine speed time variation for the same load increase (corresponding to ordered engine speed step from 37 to 43.4 rpm). Although the exhibited deviations between the simulated and measured engine speed variations, the calibrated DEM is considered sufficient to support this study scope. It must be noted though that the DEM has limitations to capture the dynamics from the engine subsystems/components thermal inertia. Another limitation pertains to DEM quantitative validation due to lack of measured data.

4. Investigated control strategies

The mode switching scenarios from Tier II to Tier III (II-III switching) and Tier III to Tier II (III-II switching) for 15% (low), 50%

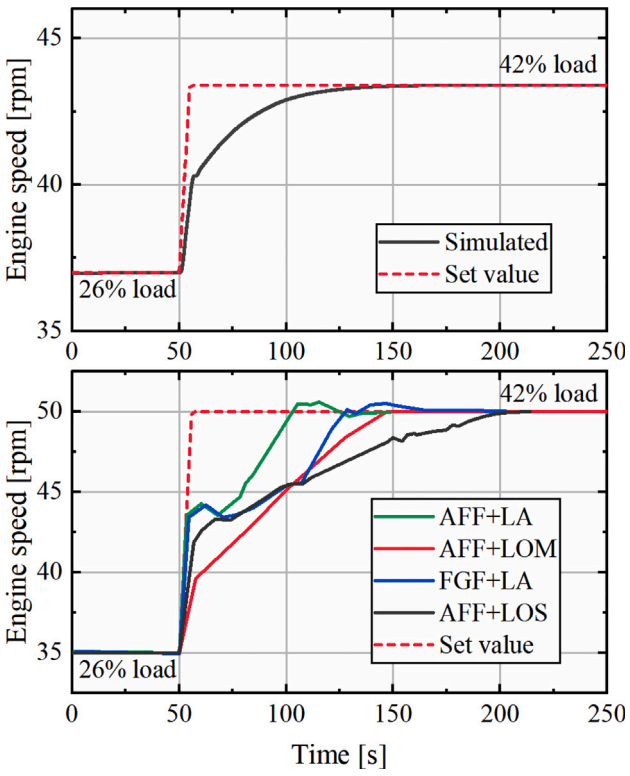

Fig. 7. Engine speed transient response comparison (top: predicted results; bottom: shipboard measurements adapted from Nielsen et al. (2017, 2018); AFF: adaptive feedforward; FGF fixed-gain feedback; LA: air/fuel ratio limiter; LOM: oxygen/fuel limiter based on oxygen model; LOS: oxygen/fuel limiter based on oxygen sensor).

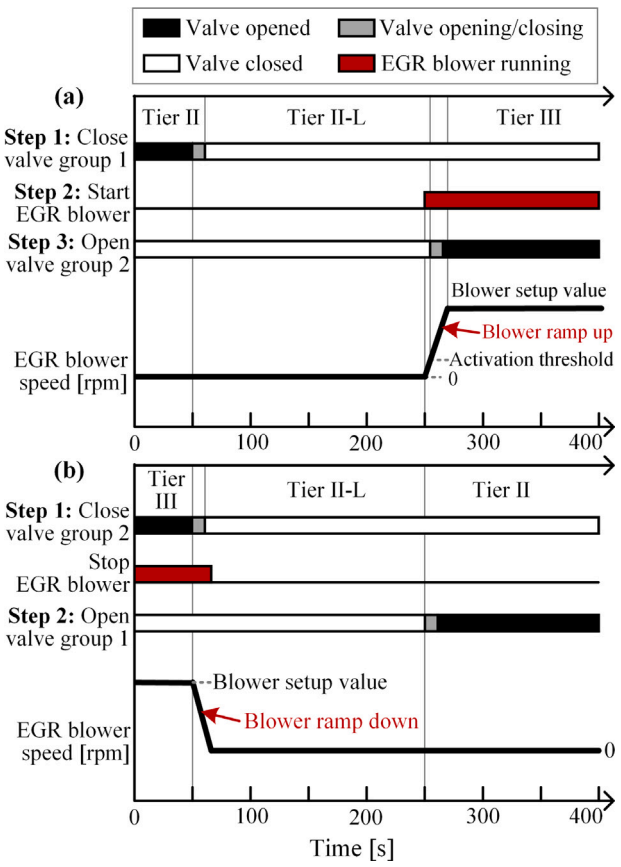

Fig. 8. Baseline control strategy steps for: (a) Tier II to Tier III mode switching; (b) Tier III to Tier II mode switching.

(medium), and 75% (high) loads are considered to investigate the impact of several control strategies and propose the recommended ones. Simulation runs with duration 400 s were performed, providing adequate time for the engine performance parameters convergence.

The baseline control strategy for the II-III mode switching consists of the following three steps, which are also illustrated in Fig. 8(a):

- Step 1: the engine operates at the Tier II mode for 50 s with open the valves of group 1 (CBV, BBV, TBV); 50–60 s: close the valves of group 1 resulting in cutting-off the small T/C and switching to Tier II-L mode.
- Step 2: the engine operates till 250 s at the Tier II-L mode; 250 s: start up the EGR blower (the EGR blower final speed depends on the engine load according to Table 2); the EGR blower speed increase rate was set to 400 rpm/s.
- Step 3: open the valves of group 2 (SOV and BTV) when the EGR blower speed exceeds the activation threshold, resulting in switching to the Tier III mode.

The baseline control strategy for the III-II mode switching consists of the following two steps, which are also shown in Fig. 8(b):

- Step 1: the engine operates at the Tier III mode for 50 s; 50–60 s: close the valves of group 2, and simultaneously shut off the EGR blower, resulting in switching to the Tier II-L mode.
- Step 2: the engine operates till 250 s at the Tier II-L mode; 250–260 s: open the valves of group 1, resulting in switching to the Tier II mode.

To address limitations (discussed in the results sections) of the baseline control strategies, several alternative control strategies are investigated. The investigated control strategies and scenarios are summarised in Table 4.

For the II-III switching, the control strategy CS1 includes skipping the Tier II-L operating mode by activating earlier the EGR branch (simultaneously or shortly after deactivating the small T/C). Several scenarios were considered with delays for the EGR blower activation of 0 s, 3 s, 5 s, and 7 s, denoted as CS1-D0, D3, D5, and D7, respectively. Step 2 for CS1 is as follows.

- Step 2: start the EGR blower at the time corresponding to 50 s and the considered time delay.

For the III-II switching, the control strategy CS2 includes skipping the Tier II-L operating mode by activating the small T/C earlier (shortly after deactivating the EGR branch). Several scenarios were considered with delays for the small T/C activation of 1 s, 3 s, 5 s, and 7 s, denoted as CS2-D1, D3, D5, and D7, respectively. Step 2 for CS2 is as follows.

- Step 2: at time of 50 s plus the delay time, open the valve group 1.

For the III-II switching, the control strategy CS3 employs the strategy CS2-D5 settings and additionally includes prolonging the EGR branch deactivation duration by adjusting the EGR blower speed decrease rate. Scenarios with different deactivation duration (DD) (to completely stop the EGR blower) of 20 s, 40 s, and 60 s, denoted as CS3-DD20, DD40 and DD60, are considered. The triggering time (TT) for closing the valve group 2 is estimated based on the EGR blower decrease rate and the valve closing duration, so that valve group 2 is fully closed when the EGR blower switches off. CS3 employs the following steps:

- Step 1: the engine operates at the Tier III mode for 50 s; 50 s to 50 s plus DD: deactivate the EGR blower; TT to TT plus 10 s: close the valve group 2.

Table 4
Investigated control strategies and scenarios for the engine mode switching.

Control strategy code	Mode switching	Scenarios	Steps/ characteristics	Load (%)
Baseline	II-III		According to Fig. 8(a)	25, 50, 75
Baseline	III-II		According to Fig. 8(b)	25, 50, 75
CS1	II-III	CS1-D0 CS1-D3 CS1-D5 CS1-D7	Baseline considering delays for the EGR blower activation of 0 s, 3 s, 5 s, and 7 s after the 50rh s	75
CS2	III-II	CS2-D1 CS2-D3 CS2-D5 CS2-D7	Baseline considering delays for the small T/C activation of 1 s, 3 s, 5 s, and 7 s after the 50rh s	75
CS3	III-II	CS3-DD20 CS3-DD40 CS3-DD60	CS2-D5 with prolonged EGR branch deactivation duration of 20 s, 40 s, and 60 s	75
CS4	III-II	CS4-A0 CS4-A3 CS4-A5 CS4-A7	CS3-DD20 with advancing the activation time of the small T/C by 0 s, 3 s, 5 s and 7 s	75
CS5	III-II	CS5-CAD0 CS5-CAD1 CS5-CAD2 CS5-CAD3	Baseline with delayed start of injection (SOI) by 0 °CA, 1 °CA, 2 °CA, and 3 °CA prior to EGR system deactivation	75
CS6	III-II	CS6-D10 CS6-D20 CS6-D30	CS5-CAD2 with prolonged EGR branch deactivation duration of 10 s, 20 s, and 30 s	75

- Step 2: at time of TT plus the delay time, open the valve group 1. The delay time was set to 5 s, as for the control strategy CS2-D5.

For the III-II switching, the control strategy CS4 employs the steps of CS3-DD20, and additionally considers advancing the activation time of the small T/C by 0 s, 3 s, 5 s and 7 s, denoted as CS4-A0, A3, A5 and A7. As CS3-DD20 considers 5 s delay for the small T/C activation, scenarios A0 to A7 include delays for the small T/C activation (switching on valve group 1) of 5 s, 2 s, 0 s and –2 s relative to the triggering time (TT) for closing the valve group 2. Step 2 for CS4 is as follows.

- Step 2: at time equal to TT plus the delay time minus the advance time, open the valve group 1.

For switching from Tier III to Tier II-L (III-IIL switching), the control strategy CS5 considers delayed start of injection (SOI) by 0 °CA, 1 °CA, 2 °CA, and 3 °CA prior to EGR system deactivation, denoted as CS5-CAD0, CAD1, CAD2, and CAD3, respectively. Step 1 for the CS5 is as follows.

- Step 1: the engine operates at the Tier III mode with delayed SOI for 50 s; 50–60 s: close the valves of group 2, and simultaneously shut off the EGR blower, resulting in switching to the Tier II-L mode.

The control strategy CS6 additionally considers prolongation of the EGR branch deactivation period. CS6 employs the steps of CS5-CAD2 and scenarios for the EGR branch deactivation duration (DD) of 10 s, 20 s, and 30 s, denoted as CS6-DD10, DD20, and DD30, respectively. Step 1 for the CS6 is as follows.

- Step 1: the engine operates at the Tier III mode with 2 °CA SOI delay for 50 s; 50 s to 50 s plus DD: shut off the EGR blower and close the valves of group 2 when the EGR blower speed is less than 1000 rpm, resulting in switching to the Tier II-L mode.

5. Results and discussion

5.1. Tier II to Tier III mode switching

The simulation results for the II-III switching at 15% load and 75% load are shown in Figs. 9 and 10, respectively. Fig. 11 presents the trajectories of the large T/C compressor operating points.

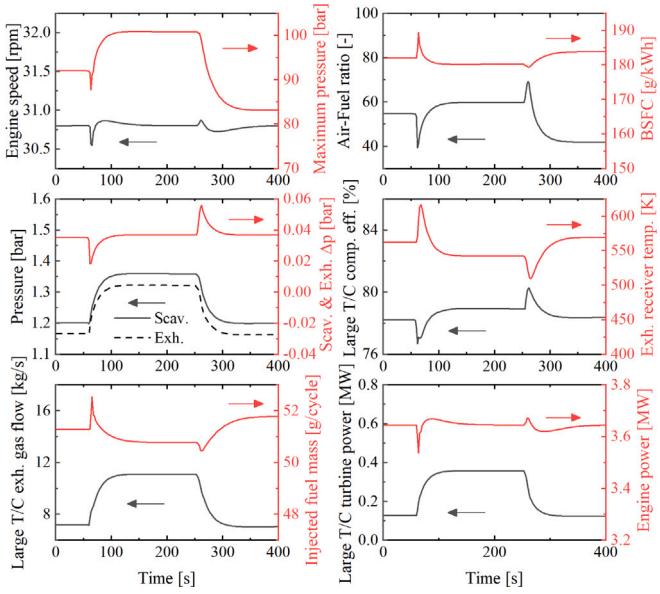

Fig. 9. Simulation results for the II-III switching at 15% load with the baseline control strategy.

The small T/C deactivation in the Tier II mode reduces the exhaust gas flow area, thereby increasing the exhaust receiver pressure and resulting in reducing the scavenging and exhaust pressure difference. This leads to reduced amount of the in-cylinder trapped air. Since the fuel injection mass varies slowly (based on the fuel rack position control), the air–fuel ratio decreases rapidly, resulting in the overshoot of the exhaust gas receiver temperature. Subsequently, the cylinder maximum pressure decreases, which in turn reduces the engine output power and speed, as well as increases the engine fuel consumption. The engine BSFC at 15% and 75% loads increased by up to about 8 g/kWh and 16 g/kWh respectively, while the exhaust receiver temperature increased by up to 55 K and 135 K, respectively.

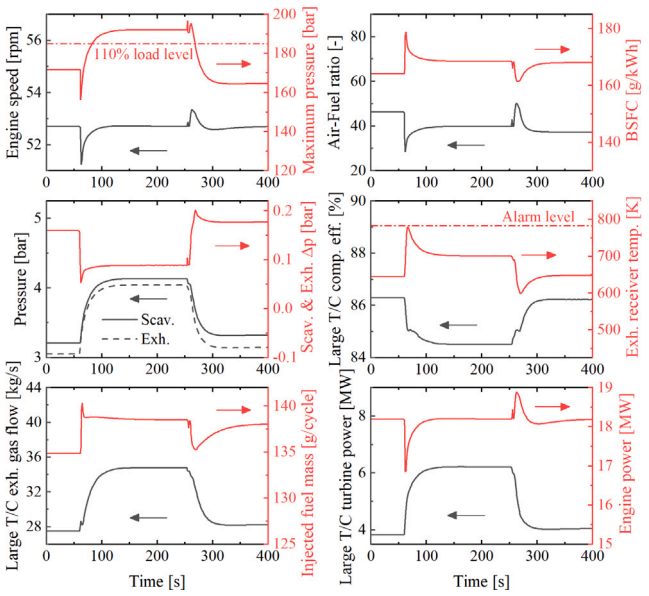

Fig. 10. Simulation results for the II-III switching at 75% load with the baseline control strategy.

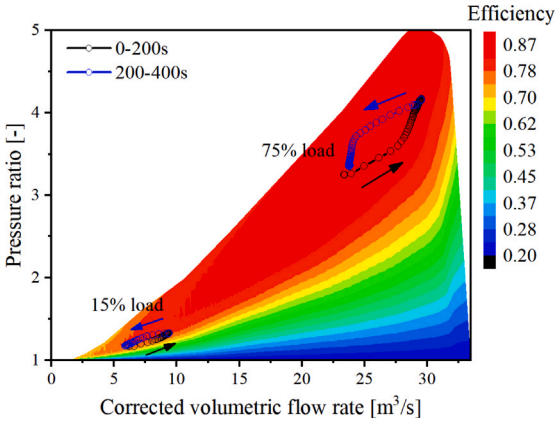

Fig. 11. Large T/C compressor operating points trajectories during the II-III switching with the baseline control strategy.

It is inferred that, compared with the low load operation, the small T/C deactivation has a greater temporal impact on the engine performance parameters at high loads. This is attributed to the following reasons: (a) the exhaust gas flow at high loads is much greater compared to low loads; therefore, the small T/C deactivation leads to the greater exhaust gas flow reduction; (b) the auxiliary blower is activated at 15% load, mitigating the scavenging efficiency deterioration to a certain extent.

The increase of the exhaust receiver temperature and pressure causes the increase of the power and speed of the large T/C, which in turn increases its compressor air mass flow rate and pressure ratio. The increased scavenge receiver pressure restores the air amount entering the cylinders to some extent. To adjust the engine speed to its set value, the fuel injection mass rapidly increases under the action of the governor, thereby restoring the engine speed and power close to their values prior to the small T/C deactivation. Subsequently, the fuel injection mass decreases. The engine fuel consumption and the exhaust temperature also gradually decrease reaching their respective steady-state values.

The converged engine performance parameters for the Tier II-L mode deviate compared to their values for the Tier II mode. Among them, the exhaust receiver pressure, the scavenging receiver pressure, the cylinder maximum pressure, the power and speed of the large T/C, as well as the large T/C exhaust gas flow rate exhibited increases for both the high and low loads. For the low load, the BSFC and the exhaust receiver temperature decreased, mainly due to the increased large T/C efficiency and air–fuel ratio, which aligns with the findings in Lu et al. (2022a).

It must be noted that with the small T/C deactivated at 75% load, the peak value of the exhaust receiver temperature reaches 780 K, closely reaching the manufacturer high alarm limit. In addition, the cylinder maximum pressure exceeds the corresponding value at 110% engine load, indicating risky conditions for the engine operation. Therefore, the small T/C deactivation under the high loads should be avoided.

The simulation results for the II-III switching at 50% load employing the baseline control strategy (not presented herein for brevity) demonstrated that the peaks of the cylinder maximum pressure and the exhaust receiver temperature do not exceed their respective manufacturer limits, whereas sufficient margins exist. Therefore, the 50% load can be considered as the upper load limit for the II-III switching. However, when the engine operates in loads above 50%, the load reduction is recommended prior to the II-III switching. This may lead to increased fuel consumption and may jeopardise the manoeuvrability when the ship sails at adverse sea conditions. Therefore, refinement of the proposed switching strategy is required, as delineated to the following paragraphs.

For the II-III switching, the activation of the EGR branch in the Tier II-L mode increases the exhaust flow equivalent area and reduces the large T/C turbine mass flow, resulting in reduced exhaust receiver pressure, scavenge receiver pressure, cylinder maximum pressure, as well as large T/C power. The engine BSFC and the exhaust receiver temperature temporarily decrease, and subsequently gradually increase reaching their steady state values.

For the Tier III mode, the engine BSFC varies by +3.6 g/kWh, and −0.5 g/kWh (compared to the Tier II-L mode) at 15% and 75% loads, respectively. The activation of the EGR branch (especially at high loads) causes the temporal reduction of the large T/C compressor surge margin. However, the engine–turbocharger matching provided adequate margin to avoid compressor surging (Fig. 11). At 75% load, the large T/C surge margin varies from 25.3% to 14.9%, and then converges to 23.8%.

To retain the peak pressure and exhaust temperature within the manufacturer's limits during the II-III switching, control strategy CS1 was investigated. The simulation results for the II-III switching at 75% load employing CS1 with delays (D0 to D7) and the baseline control strategy are shown in Fig. 12.

It is deduced that control strategy CS1 can prevent exceeding the limits for the cylinder maximum pressure and exhaust temperature. The peaks of these two parameters increase with the delay time for activating the EGR branch. However, the early activation of the EGR branch leads to the higher engine speed and BSFC peaks. For scenario CS1-D5 (5 s delay), the engine speed and BSFC peaks reach similar values to the baseline II-III switching.

As the limits of the in-cylinder maximum pressure and exhaust gas temperature for loads above 75% loads are exceeded, scenarios of the control strategy CS1 with SOI retard, as well as delays and prolongation of the small T/C deactivation were also investigated. For brevity, the derived results are not presented herein. The SOI retard resulted in retaining the in-cylinder maximum pressure below its limit, however, exceeding the exhaust gas temperature limit could not be avoided. Hence, it was concluded that mode switching at high loads requires either load reduction or the use of a waste gate valve for the large T/C turbine. The later was not proposed herein to avoid the modification of the engine layout. However, it is recommended for future studies.

According to the preceding analysis, the following control strategies for the II-III switching are recommended:

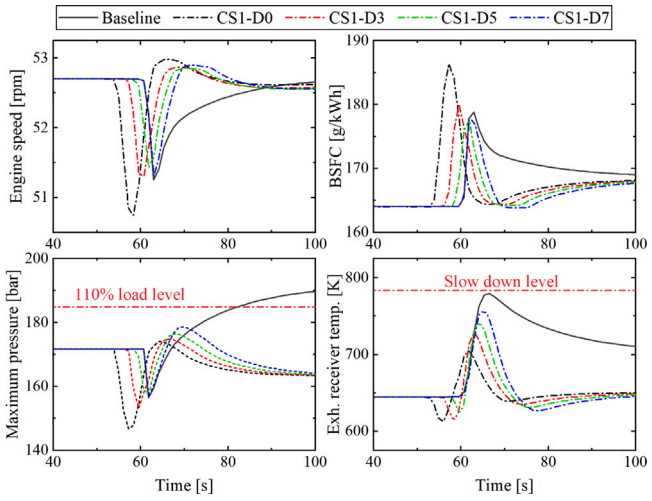

Fig. 12. Simulation results for the II-III switching at 75% load; control strategy CS1; scenarios CS1-D0 to CS1-D7 denoting 0 s to 7 s delays from the 50th s for the EGR blower activation.

(a) For loads up to 50%, the baseline control strategy shown in Fig. 8(a).
(b) For loads in the range 50%–75%, the control strategy CS1 with 5 s delay (CS1-D5).
(c) For loads greater than 75%, first load reduction to 75% and subsequently, use of the control strategy according to (b).

It should be noted that the recommended delay time and load thresholds may vary for different engine configurations and operating conditions.

5.2. Tier III to Tier II mode switching

The simulation results of the II-III switching at low (15%) and high (75%) loads are shown in Figs. 13 and 14, respectively, whereas Fig. 15 presents the large T/C compressor operating points trajectories. Comparing the II-III with the III-II operations, it can be inferred that the impact on the engine and large T/C performance and dynamic response is similar. However, since the exhaust temperature for the Tier III mode is higher than that for the Tier II mode for the same load, the EGR branch deactivation when the engine operates in the Tier III mode results in the exhaust receiver temperature overshoot, exceeding the high temperature limit. Moreover, the converged cylinder maximum pressure exceeds the corresponding value at 110% engine load. Hence, alternative control strategies for the III-II switching should be identified to prevent exceeding the manufacturer's limits.

The simulation results (not presented herein for brevity) for the III-II switching at 50% load employing the baseline control strategy showcased that the peaks of the cylinder maximum pressure and the exhaust temperature do not exceed their limits. Therefore, the engine load reduction is effective to prevent exceeding alarms when the engine operates at high loads.

To retain the peak cylinder pressure and exhaust receiver temperature within the manufacturer limits, the control strategy CS2 was investigated. The simulation results for the III-II switching at 75% load employing the CS2 and the baseline control strategies are shown in Fig. 16. It is inferred that CS2 can prevent the cylinder maximum pressure and exhaust temperature from exceeding the manufacturer's limits. However, considerable fluctuations of the engine parameters (shown in Fig. 16) occur. This is attributed to the fact that the flow rate is effectively controlled by the EGR speed when activating the EGR branch in the II-III switching, whereas the activation process of the small T/C in the III-II switching is rapid. Hence, the control strategy for

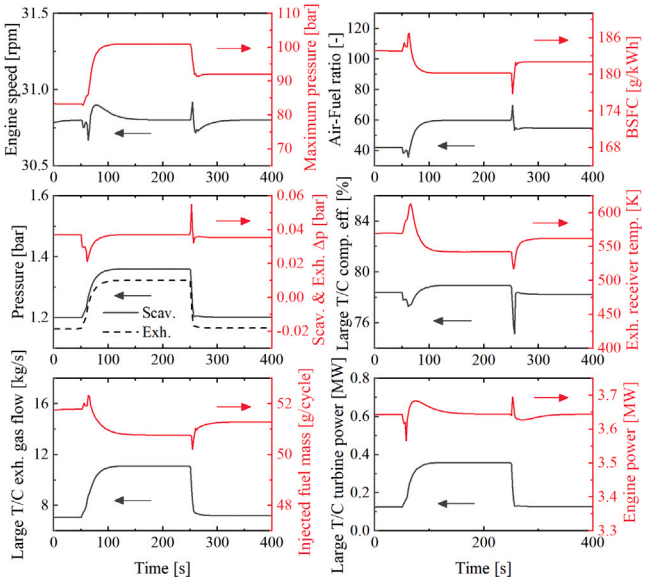

Fig. 13. Simulation results for the III-II switching at 15% load with the baseline control strategy.

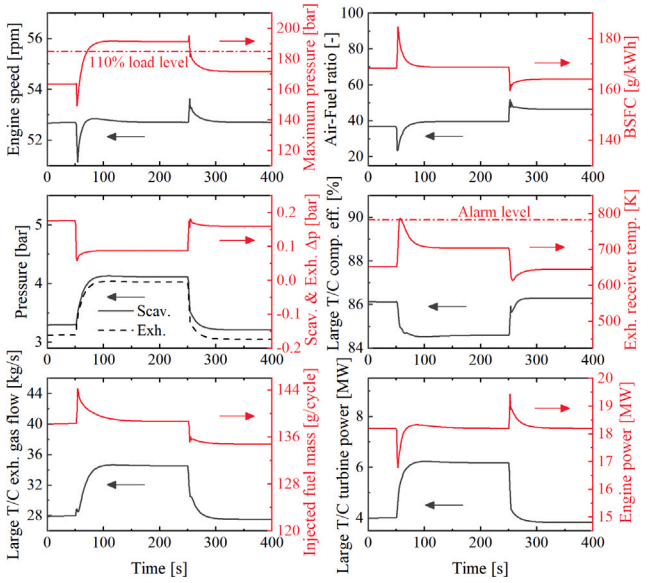

Fig. 14. Simulation results for the III-II switching at 75% load with the baseline control strategy.

activating the small T/C whilst deactivating the EGR branch requires further analysis.

As the SOV closing lasts 10 s, the early small T/C activation can cause air flowing from the small T/C compressor discharge to the exhaust gas receiver (via the SOV branch), leading to decreased air–fuel ratio and exhaust receiver temperature, as well as increased fuel consumption. It is deduced that the exhaust receiver temperature peak increases with time delay (due to the reduced charge air flow rate via the SOV branch) reaching the baseline peak values for the scenario CS2-D7 (delay of 7 s). The SOV branch air flow to the exhaust receiver causes severe fluctuations in the engine speed and BSFC; these parameters amplitudes decrease with the time delay increase. The strategy CS2-D5 exhibits relatively small fluctuations in the engine performance parameters, whereas the exhaust receiver temperature does not exceed its high limit.

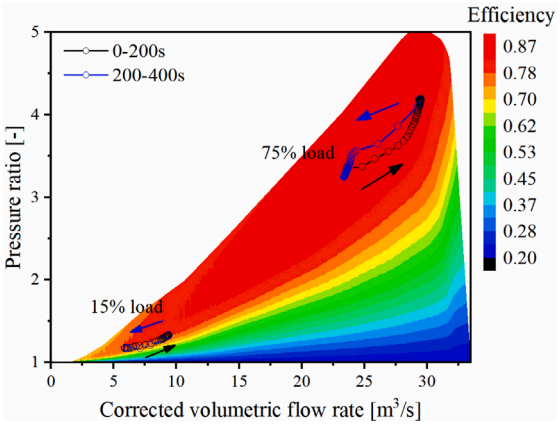

Fig. 15. Large T/C compressor operating points trajectories during the III-II switching with the baseline control strategy.

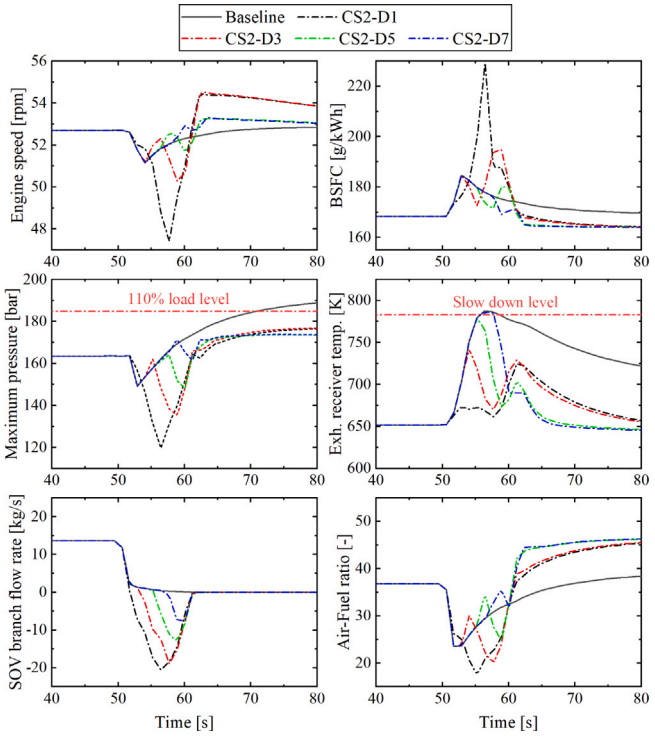

Fig. 16. Simulation results for the III-II switching at 75% load; control strategy CS2; scenarios CS2-D1 to CS2-D7.

To further reduce the exhaust receiver temperature peak and prevent these parameters severe fluctuations (caused by air back-flow in the SOV branch), the control strategy CS3 was investigated. Fig. 17 presents the simulation results for the III-II switching at 75% load using the control strategy CS3 considering different DD scenarios (corresponding to different EGR blower deactivation duration), as well as the control strategy CS2-D5 (activating the small T/C with the delay 5 s while deactivating the EGR branch).

The exhaust receiver temperature peak decreases with the DD increase, whereas the cylinder maximum pressure peak significantly increases. The other parameters fluctuations are reduced compared to CS2-D5. Although the scenario CS3-DD40 can prevent the cylinder maximum pressure and exhaust receiver temperature from exceeding the manufacturer's limits, the peaks of these parameters reach values close to their limits.

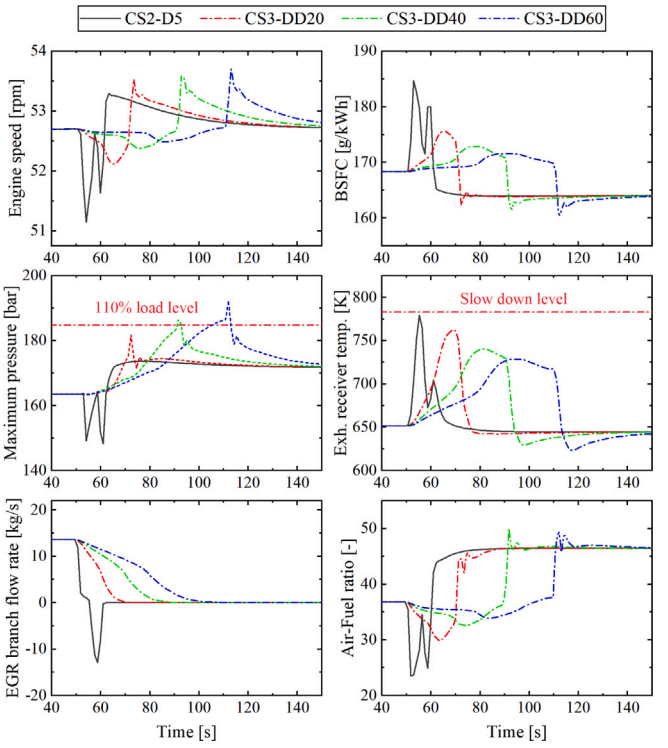

Fig. 17. Simulation results for the III-II switching at 75% load; control strategy CS3; scenarios CS3-DD20 to CS3-DD60.

As early activation of the small T/C can simultaneously reduce the cylinder maximum pressure and exhaust receiver temperature (Fig. 16), the control strategy CS4 for scenarios A0 to A7 corresponding to advancing the activation time of the small T/C is investigated. It must be noted that CS4-A0 is the same as CS3-DD20.

Fig. 18 presents the simulation results for the III-II switching at 75% load for the CS4 and CS2-D5 control strategies (activating the small T/C with the delay 5 s while deactivating the EGR branch). The peaks of the cylinder maximum pressure and exhaust receiver temperature decrease with the advance of the small T/C activation, with these two parameters remaining within the manufacturer's limits. However, further advancing the small T/C activation increases the SOV branch back-flow, which leads to the decrease of the air–fuel ratio and the cylinder maximum pressure, thereby resulting in the engine BSFC increase. CS4-A3 and A5 corresponding to 3–5 s advance of the small T/C activation resulted in exhibiting lower fuel consumption and retaining sufficient margins of the cylinder maximum pressure and exhaust temperature from their respective manufacturer limits.

Based on the preceding analysis, significant increases of the cylinder maximum pressure and exhaust gas receiver temperature are expected in loads above 75%. To address this challenge, the control strategy CS5 was investigated, with delayed SOI prior to EGR system deactivation (CAD0 to CAD3). The derived simulation results are presented in Fig. 19.

It is inferred that the cylinder maximum pressure significantly decreases with the SOI delay. When the SOI is delayed by 2 °CA (CS5-CAD2), the cylinder maximum pressure is retained well below its permissible limit, at the expense of increasing the exhaust temperature and fuel consumption. Considering that the III-IIL switching duration is short, and the mode switching does not occur frequently, the temporal increase of the fuel consumption due to the SOI delay could be acceptable. The sudden increase of the exhaust gas receiver temperature is mainly caused by the EGR blower fast shutting down, resulting in an instantaneous decrease of the cylinders air flow.

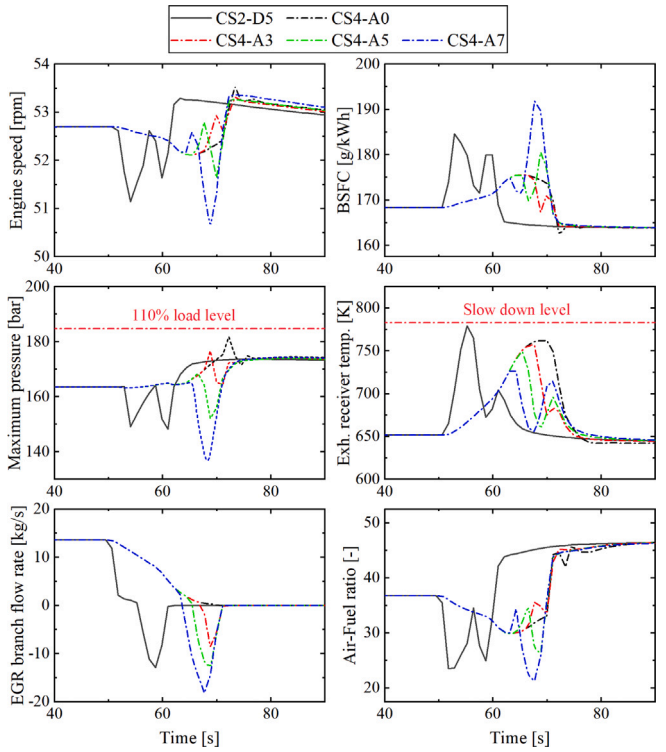

Fig. 18. Simulation results for the III-II switching at 75% load; control strategy CS4 (based on CS3-DD20); scenarios CS4-A0 to CS4-A7.

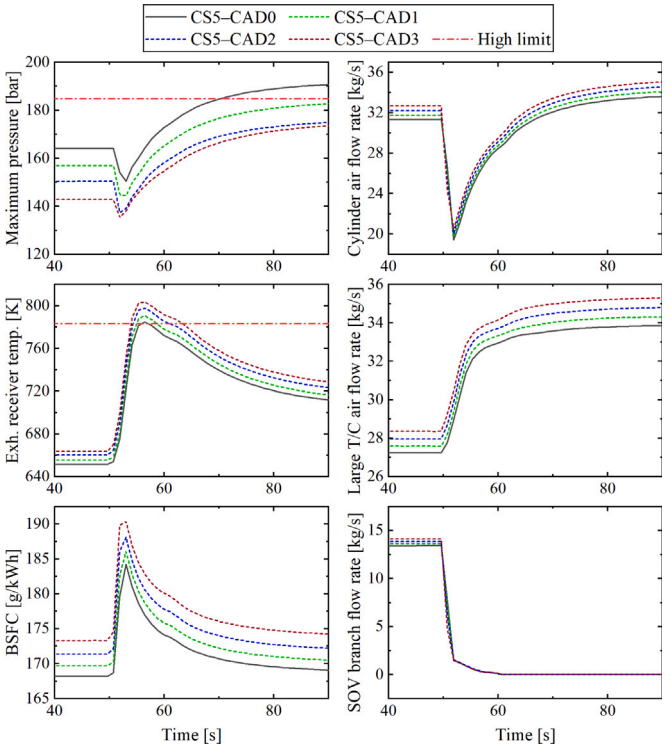

Fig. 19. Simulation results for the III-IIL switching at 75% load; control strategy CS5; scenarios CS5-CAD0 to CS5-CAD3.

To mitigate this effect, the control strategy CS6 with prolonged EGR branch deactivation duration (DD10 to DD30) was investigated. The derived simulation results are presented in Fig. 20. A significant decrease of the peak exhaust temperature is exhibited when prolonging the EGR branch deactivation. For 20 s and 30 s EGR branch deactivation duration (CS6-DD20 and CS6-DD30), the peak exhaust temperature is retained below its permissible limit. Additionally, the engine performance parameters oscillations, such as cylinder maximum pressure, BSFC, and cylinder air flow, are noticeably reduced.

Based on the preceding analysis, it is deduced that the control strategy CS6 with delayed SOI and prolonged EGR branch deactivation can effectively prevent engine parameters from exceeding the permitted limits during the III-IIL switching. Therefore, CS6 can be employed in replacing the control strategy CS4 for engine loads above 75% to avoid load reduction. For engine loads in the range 50%–75%, CS4-A3 is more effective compared to CS6-DD30, considering the estimated lower total fuel consumption during mode switching.

Based on the preceding analysis, the following control strategies for the III-II switching are proposed:

(a) For engine loads up to 50%, the baseline control strategy, as presented in Fig. 8(b).
(b) For engine loads in the range 50%–75%, the control strategy CS4-A3.
(c) For engine loads above 75%, the control strategy CS6-DD30.

It should be noted that the recommended settings may vary for different engine configurations and operating conditions.

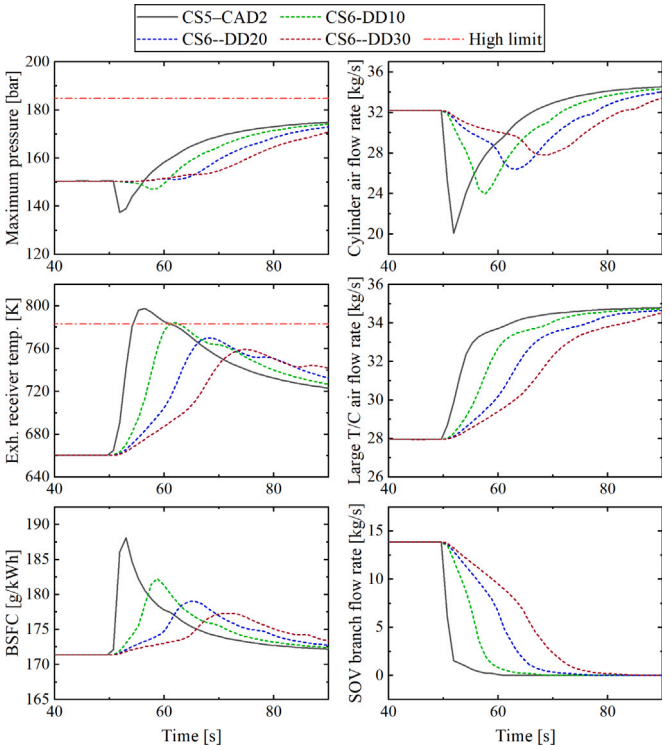

Fig. 20. Simulation results for the III-IIL switching at 75% load; control strategy CS6 (based on CS5-CAD2); scenarios CS6-DD10 to CS6-DD30.

6. Conclusions

This study investigated the mode switching for a large marine two-stroke engine with EGR and turbocharger cut-off systems (EGRTC). The dynamic engine model (DEM) was established integrating the steady-state engine model in GT-POWER and the control system model in MATLAB/Simulink. This model was first calibrated and subsequently verified using measured performance and emission parameters from the investigated engine shop tests and published data sets.

Several control strategies for the NOx emissions mode switching were proposed and tested by simulation, considering the objectives of retaining the engine operation parameters within the manufacturer's limits and avoiding high fuel consumption penalties.

The key findings of this study are summarised as follows.

- The EGR branch deactivation during the III-II switching and the small T/C deactivation during the II-III switching exhibit considerable impact on the engine and large T/C operation, resulting in exceeding the manufacturer's limits at high loads (above 75%) and high fuel consumption.
- For engine loads up to 50%, the baseline control strategies were proven effective for smooth II-III and III-II mode switching.
- For the II-III switching and loads in the range 50%–75%, the control strategy CS1-D5 with 5 s time delay for activating the EGR branch (after the small T/C deactivation) is recommended.
- For the III-II switching and loads in the range 50%–75%, the control strategy CS4-A3 is recommended; this strategy entails 2 s delay for the small T/C activation and EGR branch deactivation duration of 20 s.
- For the III-II switching at loads above 75%, the control strategy CS6-DD30 is recommended. This includes operating the engine with delayed SOI by 2 °CA, and EGR branch deactivation duration of 30 s.

This study limitations pertain to the uncertainties of the engine components submodels, especially under degradation/fouling conditions. However, the derived results provide trade-offs, which support the control design of the EGRTC engine and its systems. Future studies could consider the effects of the engine component failures and degradation on the control strategy for mode switching, the lower level control for the engine components, as well as the experimental validation of the proposed control strategies.

CRediT authorship contribution statement

Daoyi Lu: Writing – review & editing, Writing – original draft, Visualization, Software, Project administration, Methodology, Investigation, Funding acquisition, Formal analysis, Data curation, Conceptualization. **Gerasimos Theotokatos:** Writing – review & editing, Writing – original draft, Validation, Supervision, Project administration, Methodology, Formal analysis, Conceptualization. **Keying Cui:** Validation, Software, Methodology.

Declaration of competing interest

The authors declare that they have no known competing financial interests or personal relationships that could have appeared to influence the work reported in this paper.

Acknowledgements

This work was supported by the National Key R&D Program of China (Grant number: 2022YFB4301403).

References

Alegret, G., Llamas, X., Vejlgaard-Laursen, M., & Eriksson, L. (2015). Modeling of a large marine two-stroke diesel engine with cylinder bypass valve and EGR system. *IFAC-PapersOnLine*, *48*(16), 273–278. http://dx.doi.org/10.1016/j.ifacol.2015.10.292.

Bowman, C. T. (1973). Kinetics of nitric oxide formation incombustion processes. *Vol. 14*, In *Symposium (international) on combustion* (pp. 729–738). Elsevier, http://dx.doi.org/10.1016/S0082-0784(73)80068-2.

Chen, S., & Flynn, P. (1965). *Development of a single cylinder compression ignition research engine*: *SAE Technical Paper 650733*, (p. 14). SAE, http://dx.doi.org/10.4271/650733.

Gamma, T. (2016a). *Engine performance application manual*: *Technical Report*, Westmont, IL, USA: Gamma Technologies.

Gamma, T. (2016b). *Flow theory manual*: *Technical Report*, Westmont, IL, USA: Gamma Technologies.

Gamma, T. (2016c). *GT-SUITE manual*: *Technical Report*, Westmont, IL, USA: Gamma Technologies.

Hiraoka, N., Miyanagi, A., Kuroda, K., Ito, K., Nakagawa, T., & Ueda, T. (2016). The world's first onboard verification test of UE engine with low pressure EGR complied with imo's NOx tier III regulations. *Mitsubishi Heavy Industries Technical Review*, *53*(2), 40–47.

Hountalas, D. T., Raptotasios, S. I., & Zannis, T. C. (2013). Implications of exhaust gas, CO2, and N2 recirculation on heavy-duty diesel engine performance, soot, and NO emissions: A comparative study. *Energy & Fuels*, *27*(8), 4910–4929. http://dx.doi.org/10.1021/ef400289w.

IMO (2008). *Annex VI of MARPOL 73/78, Regulations for the Prevention of Air Pollution from Ships and NOx Technical Code*: *Technical Report*, London, UK: International Maritime Organization.

Jeon, J., & Theotokatos, G. (2024). A framework to assure the trustworthiness of physical model-based digital twins for marine engines. *Journal of Marine Science and Engineering*, *12*(4), 595. http://dx.doi.org/10.3390/jmse12040595.

Kaltoft, J., & Preem, M. (2013). Challenge of environmentally-friendly low emission system to tier 3 for two-stroke diesel engines. In *Proceedings of the 27th CIMAC world congress*. Shanghai, China.

Liu, W., Long, Y., Liu, S., Zhou, Y., Tong, X., Yin, Y., et al. (2022). Commercial SCR catalyst modified with different noble metals (Ag, Pt, Pd) to efficiently remove slip ammonia and NOx in the flue gas. *Journal of the Taiwan Institute of Chemical Engineers*, *138*, Article 104472. http://dx.doi.org/10.1016/j.jtice.2022.104472.

Loganx (2019). *Super Container Ship*: *Technical Report*, Cranes and Machines, Available online at https://gruasyaparejos.com/en/port-crane/super-container-ship/.

Lou, D., Lou, G., Wang, B., Fang, L., & Zhang, Y. (2021). Effect of LP-EGR on the emission characteristics of GDI engine. *Machines*, *10*(1), 7. http://dx.doi.org/10.3390/machines10010007.

Lu, D., Theotokatos, G., Zhang, J., Tang, Y., Gan, H., Liu, Q., et al. (2021). Numerical investigation of the high pressure selective catalytic reduction system impact on marine two-stroke diesel engines. *International Journal of Naval Architecture and Ocean Engineering*, *13*, 659–673. http://dx.doi.org/10.1016/j.ijnaoe.2021.09.003.

Lu, D., Theotokatos, G., Zhang, J., Zeng, H., & Cui, K. (2022a). Comparative assessment and parametric optimisation of large marine two-stroke engines with exhaust gas recirculation and alternative turbocharging systems. *Journal of Marine Science and Engineering*, *10*(3), 351. http://dx.doi.org/10.3390/jmse10030351.

Lu, D., Theotokatos, G., Zhang, J., Zeng, H., & Cui, K. (2022b). Parametric investigation of a large marine two-stroke diesel engine equipped with exhaust gas recirculation and turbocharger cut out systems. *Applied Thermal Engineering*, *200*, Article 117654. http://dx.doi.org/10.1016/j.applthermaleng.2021.117654.

MAN (2008). *Exhaust gas emission control today and tomorrow: application on MAN B&W two-stroke marine diesel engines*: *Technical Report*, Copenhagen, Denmark: MAN Diesel & Turbo.

MAN (2015). *Tier III programme status and outlook*: *Technical Report*, Copenhagen, Denmark: MAN Energy Solutions.

MAN (2018). *MAN B&W G80ME-C9.5-TII project guide electronically controlled two-stroke engines*: *Technical Report*, Copenhagen, Denmark: MAN Energy Solutions.

MAN (2020). *EGR offered for dual-fuel ME-GA engine*: *Technical Report*, Copenhagen, Denmark: MAN Energy Solutions.

Mandra, J. O. (2022). *WinGD scoops 1st on-engine iCER order*: *Technical Report*, OFFSHORE ENERGY, Available online at https://www.offshore-energy.biz/wingd-scoops-1st-on-engine-icer-order/.

Nakagawa, T., Ito, K., & Edo, K. (2019). The latest technologies of NOx emission control for UE engines. In *Proceedings of the 29th CIMAC world congress*. Vancouver, Canada.

Nakagawa, T., Onishi, I., Nakao, S., Hosono, T., & Nishiyama, A. (2016). Challenge of environmentally-friendly low emission system to tier 3 for two-stroke diesel engines. In *Proceedings of the 28th CIMAC world congress*. Helsinki, Finland.

Nielsen, K. V., Blanke, M., Eriksson, L., & Vejlgaard-Laursen, M. (2017). Adaptive feed-forward control of exhaust recirculation in large diesel engines. *Control Engineering Practice*, *65*, 26–35. http://dx.doi.org/10.1016/j.conengprac.2017.05.003.

Nielsen, K. V., Blanke, M., Eriksson, L., & Vejlgaard-Laursen, M. (2018). Marine diesel engine control to meet emission requirements and maintain maneuverability. *Control Engineering Practice*, *76*, 12–21. http://dx.doi.org/10.1016/j.conengprac.2018.03.012.

Park, S., Cho, J., Park, J., & Song, S. (2017). Numerical study of the performance and NOx emission of a diesel-methanol dual-fuel engine using multi-objective Pareto optimization. *Energy*, *124*, 272–283. http://dx.doi.org/10.1016/j.energy.2017.02.029.

Rao, V., & Honnery, D. (2013). A comparison of two NOx prediction schemes for use in diesel engine thermodynamic modelling. *Fuel*, *107*, 662–670. http://dx.doi.org/10.1016/j.fuel.2013.01.071.

Schneiter, D. (2015). *Tier III Programme Technical Position, Status and Outlook: Technical Report*, Interlaken, Switzerland: Winterthur Gas & Diesel.

Shen, H. S. (2020). *Research on the modeling methodology of marine large-scale two-stroke diesel engine and compressor* (Ph.D. thesis), Dalian, China: Dalian Maritime University.

Shen, H., Zhang, J., Yang, B., & Jia, B. (2020). Development of a marine two-stroke diesel engine MVEM with in-cylinder pressure trace predictive capability and a novel compressor model. *Journal of Marine Science and Engineering*, *8*(3), 204. http://dx.doi.org/10.3390/jmse8030204.

Stoumpos, S., & Theotokatos, G. (2020). Multiobjective optimisation of a marine dual fuel engine equipped with exhaust gas recirculation and air bypass systems. *Energies*, *13*(19), 5021. http://dx.doi.org/10.3390/en13195021.

Vignesh, R., & Ashok, B. (2020). Critical interpretative review on current outlook and prospects of selective catalytic reduction system for De-NOx strategy in compression ignition engine. *Fuel*, *276*, Article 117996. http://dx.doi.org/10.1016/j.fuel.2020.117996.

Wang, D., Shi, L., Zhu, S., Liu, B., Qian, Y., & Deng, K. (2020). Numerical and thermodynamic study on effects of high and low pressure exhaust gas recirculation on turbocharged marine low-speed engine. *Applied Energy*, *261*, Article 114346. http://dx.doi.org/10.1016/j.apenergy.2019.114346.

Wang, D., Zhang, H., Qian, Y., & Deng, K. (2022). Experimental energy and exergy analysis of turbocharged marine low-speed engine with high pressure exhaust gas recirculation. *Fuel*, *323*, Article 124360. http://dx.doi.org/10.1016/j.fuel.2022.124360.

Wang, Z., Zhou, S., Feng, Y., & Zhu, Y. (2017). Research of NOx reduction on a low-speed two-stroke marine diesel engine by using EGR (exhaust gas recirculation)–CB (cylinder bypass) and EGB (exhaust gas bypass). *International Journal of Hydrogen Energy*, *42*(30), 19337–19345. http://dx.doi.org/10.1016/j.ijhydene.2017.06.009.

Woschni, G. (1967). *A universally applicable equation for the instantaneous heat transfer coefficient in the internal combustion engine*: *SAE Technical paper 670931*, SAE, http://dx.doi.org/10.4271/670931.

You, J., Liu, Z., Wang, Z., Wang, D., & Xu, Y. (2020). Experimental analysis of inert gases in EGR on engine power and combustion characteristics in a stoichiometric dual fuel heavy-duty natural gas engine ignited with diesel. *Applied Thermal Engineering*, *180*, Article 115860. http://dx.doi.org/10.1016/j.applthermaleng.2020.115860.

Zheng, M., Reader, G. T., & Hawley, J. G. (2004). Diesel engine exhaust gas recirculation—-A review on advanced and novel concepts. *Energy Conversion and Management*, *45*(6), 883–900. http://dx.doi.org/10.1016/S0196-8904(03)00194-8.